Excitation of the Madden-Julian Oscillation in Response to Transient Ocean Warming in SPCAM

Yu Liang, Alexey V. Fedorov

Geophysical Research Letters

RESEARCH LETTER
10.1029/2022GL100853

Key Points:

- In Super-parameterized Community Atmosphere Model, a robust Madden-Julian oscillation (MJO) event is excited in response to transient sea surface warming in the equatorial Indian Ocean
- Longwave and latent heat flux anomalies are predominantly responsible for the MJO excitation, which however oppose its eastward propagation
- Advection of moist static energy generally weakens the MJO amplitude but contributes to its eastward propagation

Supporting Information:

Supporting Information may be found in the online version of this article.

Correspondence to:

Y. Liang,
yu.liang@yale.edu

Citation:

Liang, Y., & Fedorov, A. V. (2022). Excitation of the Madden-Julian oscillation in response to transient ocean warming in SPCAM. *Geophysical Research Letters*, *49*, e2022GL100853. https://doi.org/10.1029/2022GL100853

Received 16 AUG 2022
Accepted 28 OCT 2022

Excitation of the Madden-Julian Oscillation in Response to Transient Ocean Warming in SPCAM

Yu Liang[1] and Alexey V. Fedorov[1,2]

[1]Department of Earth and Planetary Sciences, Yale University, New Haven, CT, USA, [2]LOCEAN/IPSL, Sorbonne University, Paris, France

Abstract Recent studies have suggested that the Madden-Julian oscillation (MJO) could be generated as part of atmospheric adjustment to localized equatorial heating in models properly resolving moist convection. Here we use the Super-parameterized Community Atmosphere Model (SPCAM) to study atmospheric response to transient sea surface warming in the equatorial Indian Ocean, which leads to the excitation of an MJO event, robust across different experiments, in addition to the expected equatorial Rossby and Kelvin waves. A moist static energy (MSE) budget analysis suggests that longwave and surface turbulent latent heat flux anomalies are predominantly responsible for the MJO excitation; however, these terms oppose its eastward propagation. In contrast, advection of MSE generally weakens the MJO amplitude, but contributes to its eastward propagation. These results highlight the role of the MJO in the moist atmospheric adjustment to localized tropical heating, with implications for the MJO mechanisms and prediction.

Plain Language Summary The Madden-Julian oscillation (MJO) is a large-scale eastward-propagating precipitation system in the tropical atmosphere, which has strong impacts on weather and climate in the tropics and beyond. Here we investigate the excitation of an MJO event in response to a localized transient sea surface warming in the equatorial Indian Ocean using the Super-parameterized Community Atmosphere Model (SPCAM), a numerical atmospheric general circulation model that simulates cumulus convection explicitly. We find that in addition to equatorial waves expected from the classical theories of equatorial atmospheric dynamics, a robust MJO event is generated in response to the imposed sea surface warming. An energy budget analysis is conducted to understand the mechanisms for initiation and eastward propagation of this MJO event. The study highlights the importance of the MJO in the atmospheric response to tropical heating, with implications for the MJO prediction, as our results suggest that warm sea surface temperature anomalies in the equatorial Indian Ocean can initiate MJO events.

1. Introduction

In the classical studies of Matsuno (1966), Gill (1980), Heckley and Gill (1984), among many others using a dry shallow water model on the equatorial β-plane, the response of the tropical atmosphere to a localized equatorial heating anomaly could be described by low-level easterly winds associated with Kelvin waves to the east, and Rossby cyclonic flow to the west of the imposed anomaly. Once the heating is turned off, this so-called Matsuno-Gill pattern would then disintegrate and become propagating equatorial Kelvin and Rossby waves (Haertel, 2020). The generation of Kelvin and Rossby waves from localized atmospheric heating was also demonstrated in a dry general circulation model (GCM) by Jin and Hoskins (1995). Although the equatorial heating is usually caused by vapor condensation in moist convection (Yanai et al., 1973), it is often treated as mass sink in such "dry" models. However, when vapor condensation is explicitly included in a shallow water model, studies have found that the adjustment of a localized large-scale pressure anomaly (Rostami & Zeitlin, 2020), or a localized heat source at the equator (Vallis, 2021), could induce an eastward-propagating disturbance arguably resembling the Madden-Julian oscillation (MJO, Madden & Julian, 1972), although only the crudest features of the MJO could be captured.

Recently, using a Lagrangian atmospheric general circulation model reproducing a fairly realistic MJO, Liang, Fedorov, Zeitlin, and Haertel (2021) have found that robust MJO events could be excited in response to warm sea surface temperature (SST) perturbations of various scales and magnitudes imposed in the equatorial Indian Ocean. These modeling results highlighted the importance of moist convection in the MJO dynamics, as suggested by

many previous studies (e.g., Adames & Kim, 2016; Raymond & Fuchs, 2009; Sobel & Maloney, 2013), and more importantly, the critical role of the MJO in the moist atmospheric adjustment.

Characterized by a large-scale eastward-propagating precipitation envelope, the MJO is the dominant intraseasonal mode in the tropical atmosphere (Madden & Julian, 1972; Wheeler & Kiladis, 1999). The MJO usually originates in the tropical Indian Ocean, propagates eastward across the Maritime Continent, reaches the West Pacific, and dissipates around the dateline. It can modulate tropical cyclogenesis (e.g., Liebmann et al., 1994; Maloney & Hartmann, 2000), interact with El Niño (e.g., Kessler & Kleeman, 2000; Liang & Fedorov, 2021; Liang, Fedorov, & Haertel, 2021; McPhaden, 1999), trigger the onset of the Asian and Australian monsoons (e.g., Hendon & Liebmann, 1990; Lau & Phillips, 1986), and affect weather extremes outside the tropics (e.g., Higgins et al., 2000; Jones et al., 2004). Given its impacts on the global climate and weather systems, and its quasi-periodic nature, the MJO has been considered a major source of predictability for subseasonal to seasonal weather forecasts (e.g., Waliser, 2005). Nevertheless, despite strong efforts in the past several decades, realistic simulation and prediction of the MJO remain challenging in state-of-the-art numerical models (Kim et al., 2018; Klingaman et al., 2015), calling for a better understanding of the MJO dynamics, including the mechanisms for its onset and eastward propagation.

One feature sometimes observed before the initiation of an MJO event, especially if it follows another MJO event, is an anomalous warming of 1–3 K of the equatorial Indian Ocean (DeMott et al., 2015; Flatau et al., 1997; Matthews, 2008; Moum et al., 2014; Shinoda et al., 1998). These warm SST anomalies could enhance the boundary layer moisture convergence (Rydbeck & Jensen, 2017), and increase latent heat flux during the MJO convective growth (DeMott et al., 2015), contributing to the event onset. Note that other processes, such as horizontal moisture advection, have also been suggested important in the successive MJO initiation (Li et al., 2015; Sobel et al., 2014; Zhao et al., 2013).

Although a number of studies have shown that adding intraseasonal SST anomalies to AGCMs would enhance MJO-like variability (Stan, 2018; Woolnough et al., 2001), previous attempts to simulate MJO initiation in response to a transient ocean warming were generally not successful (Maloney & Hartmann, 2000; Nakajima et al., 2004), except more recently in Liang, Fedorov, Zeitlin, and Haertel (2021) who used a Lagrangian atmospheric model (LAM, Haertel et al., 2014, 2017). In the present study, we will use the Super-parameterized Community Atmosphere Model (SPCAM, Khairoutdinov & Randall, 2001) to simulate excitation of an MJO event in response to a transient idealized SST warming in the equatorial Indian Ocean, and investigate mechanisms for the onset and eastward propagation of this event.

The purpose of this study is two-fold. First, using a GCM of higher model hierarchy we will validate the modeling results in Liang, Fedorov, Zeitlin, and Haertel (2021). Compared to LAM, SPCAM utilizes more realistic cloud microphysics, radiation transfer, and land model. It has been known to simulate realistic MJOs (Hannah et al., 2015; Klingaman et al., 2015, see also the wavenumber-frequency spectra in Figure S1 in Supporting Information S1), and has been used as a benchmark for conventional GCM cumulus parameterization schemes (Rasp et al., 2018). Second, Liang, Fedorov, Zeitlin, and Haertel (2021) conducted a moisture budget analysis to understand the mechanisms of the excited MJO's eastward propagation, so that the role of cloud-radiation feedback, suggested as a key instability mechanism for the MJO in some studies (Andersen & Kuang, 2012; Raymond, 2001; Sobel & Maloney, 2013), could not be investigated. Here, instead, we will analyze the moist static energy (MSE) budget, which incorporates the radiation effects, in order to examine the mechanisms not only for the eastward propagation, but also for the onset of the excited MJO in SPCAM.

2. Experiment Setup

We use the SPCAM, which is a part of the Community Earth System Model version 2.1.0 (CESM2) developed at National Center for Atmospheric Research (Danabasoglu et al., 2020). Different from conventional cumulus parameterization, SPCAM utilizes an embedded two-dimensional cloud-resolving model to simulate subgrid-scale convection. It is based on the System for Atmospheric Modeling (Khairoutdinov & Randall, 2003), where a single-moment bulk microphysics scheme is used. For all simulations, SPCAM has a horizontal resolution of $1.8° \times 2.5°$, and 26 vertical levels; the model output is saved every 3 hr. The Control experiment is forced by the March climatological SST, sea ice concentration and insolation, estimated for 1995–2005, and is integrated for four years. We choose March to be consistent with Liang, Fedorov, Zeitlin, and Haertel (2021), and

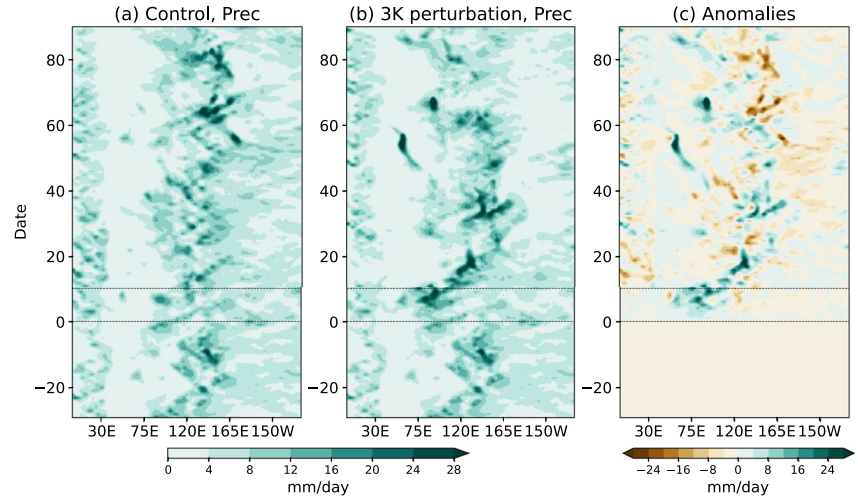

Figure 1. Hovmöller diagrams of equatorially averaged (10°N–10°S) precipitation in the (a) Control and (b) 3K perturbation experiments, and (c) precipitation anomalies in the 3K perturbation experiment relative to the Control, which hereafter are used to indicate the excited Madden-Julian oscillation (MJO) event. Day 0 indicates the date when the warm sea surface temperature (SST) perturbation is first added, lasting for 10 days before it's turned off. A clear MJO event is observed in response to the transient SST perturbation in (b). A secondary event originating over the Maritime Continent can also be seen starting on day 30.

also because we impose a symmetric heating with respect to the equator and typically the MJO is most symmetric in March.

For the perturbation experiment, we restart the Control simulation with initial conditions on day 231, year 3 (Figure 1a, Figure S2a in Supporting Information S1), when the MJO is inactive (i.e., no coherent eastward propagation of intraseasonal precipitation anomalies is seen), and add an idealized Gaussian-shape warm SST perturbation (SST_{pert}, Equation 1) to the climatological March SST boundary condition. Day 231, year 3 is then referred to as day 0. This SST perturbation has a maximum amplitude of 3K (Figure S3 in Supporting Information S1), and lasts for 10 days, after which the climatological March SST is used to force the model for another 95 days. Note that this SST perturbation is similar to one of the perturbations used by Liang, Fedorov, Zeitlin, and Haertel (2021), and is comparable to the warmest SST perturbations observed before the initiation of some MJO events (DeMott et al., 2015; Moum et al., 2014).

$$SST_{pert} = 3°C \times \exp\left(-(\text{longitude} - 75°E)^2/2/30°^2\right) \times \exp\left(-\text{latitude}^2/2/10°^2\right) \quad (1)$$

3. Results

3.1. MJO Generation

In response to the imposed SST perturbation, a clear MJO-like precipitation disturbance develops in this 3K perturbation experiment (Figure 1). The excited MJO event originates in the central equatorial Indian Ocean, propagates eastward at a speed of about 6 m/s, and dissipates in the western Pacific. The speed of propagation is computed by estimating the eastward shift of positive precipitation anomalies along the equator between days 8 and 16 (see Figures 2b and 2d). A secondary MJO event also appears to emerge over the Maritime Continent on day 30, and propagates toward the dateline, similar to the findings in Liang, Fedorov, Zeitlin, and Haertel (2021), although its eastward propagation is less clear in the 20-100-day bandpass filtered field (Figure S2b in Supporting Information S1).

Hereafter, we plot anomalous fields (e.g., precipitation, winds) in the 3K perturbation experiment relative to the Control, in reference to day 0, to indicate the excited MJO event. Snapshots of anomalous precipitation and wind vectors at 200 hPa are shown in Figure 2; anomalous wind fields at 850 hPa are shown in Figure S4 in Supporting Information S1 for reference. To retain only the planetary-scale features of the excited MJO event, all anomalous fields in this study are smoothed by applying a 1-2-1 filter 24 times zonally and three times meridionally, which reduces the amplitude of the signal at zonal wavenumbers 11 and higher by over 70%. A smoother field could be obtained by applying this filter even more times, but the main conclusion of this paper would not be affected.

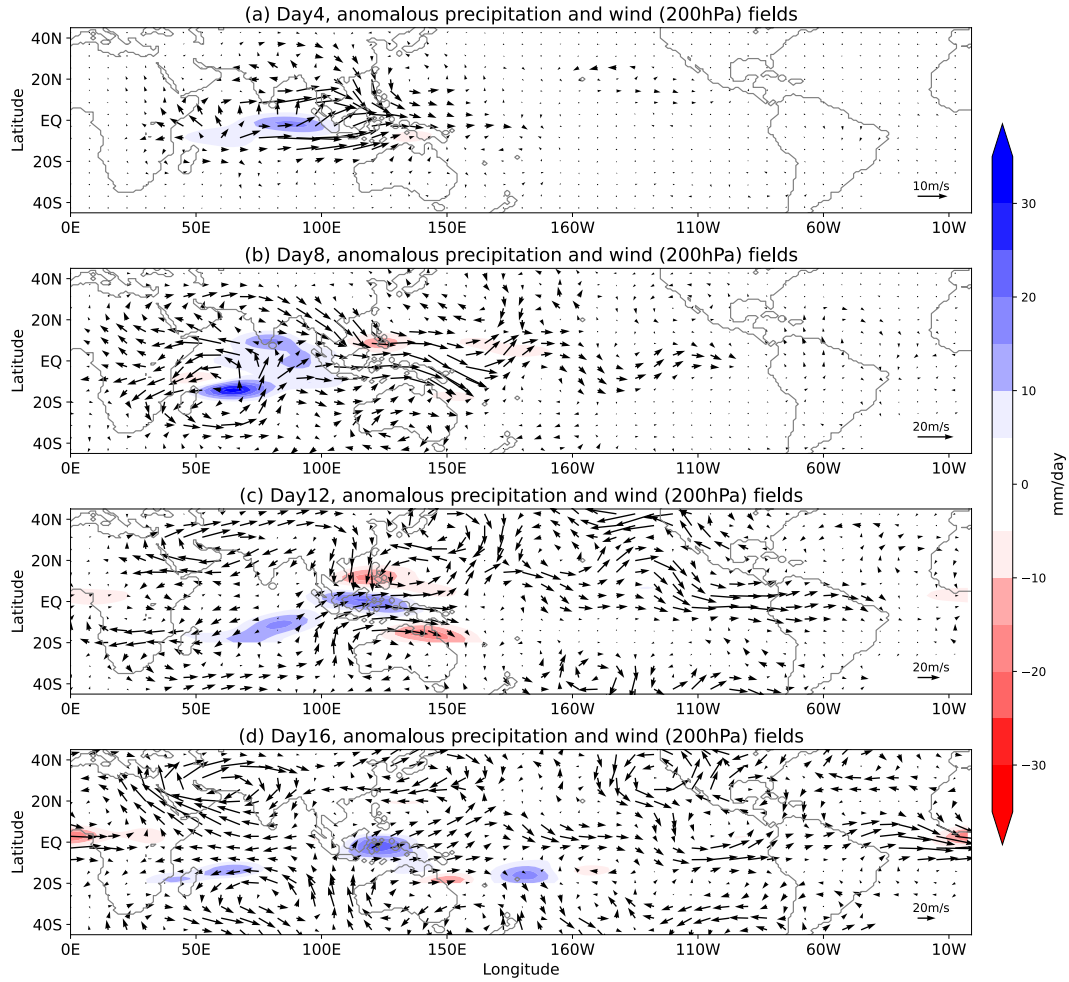

Figure 2. Snapshots of precipitation and upper-level wind vector anomalies in the 3K perturbation experiment relative to the Control on days 4, 8, 12, and 16. The excited Madden-Julian oscillation (MJO) event, marked by positive precipitation anomalies on the equator, starts to propagate eastward on day 8. The upper-level quadrupole circulation typical of the MJO can be discerned on days 12 and 16. Note that for clarity, we only show precipitation anomalies within 20°N/S.

As shown in Figures 2a and 2b, on days 4 and 8, after the SST perturbation was first added, basin-wide positive precipitation anomalies develop in the central-eastern equatorial Indian Ocean over the warm SST perturbation. A Gill-type response in the upper troposphere, indicated by two anticyclonic Rossby gyres to the west of the enhanced precipitation and equatorial Kelvin wave westerlies to the east, is clearly observed on day 8. In the lower troposphere (Figure S4 in Supporting Information S1), two cyclonic Rossby gyres are confined closer to the equator, consistent with the observed MJO structure (Zhang, 2005). On day 12, the center of positive precipitation anomalies has moved to the Maritime Continent, while the Kelvin wave font (westerlies) has already reached the Atlantic. The upper-level quadrupole circulation—a salient feature of the MJO (Kiladis et al., 2005)—can also be discerned at this time (Figure 2c). On day 16, positive precipitation anomalies along the equator start to weaken, but the quadrupole circulation is still evident (Figure 2d). The excited MJO event finally dissipates when it reaches the western equatorial Pacific on day 18, and the anomalous fields are not shown thereafter.

To examine the upper-level wind response more closely, in Figure 3 we plot the Hovmöller diagram of zonal wind anomalies at 200 hPa, 1°N. Indicated by the upper-level divergence center, the MJO slowly propagates eastward, while westward propagation of the Rossby wave front (easterly anomalies) and eastward propagation of the Kelvin wave front (westerly anomalies) can also be distinctly observed. This differs from the atmospheric response to a localized tropical heating in a dry GCM (Jin & Hoskins, 1995), where only Rossby and Kelvin wave fronts were observed. The Rossby and Kelvin wave fronts in the current study propagate at a speed of

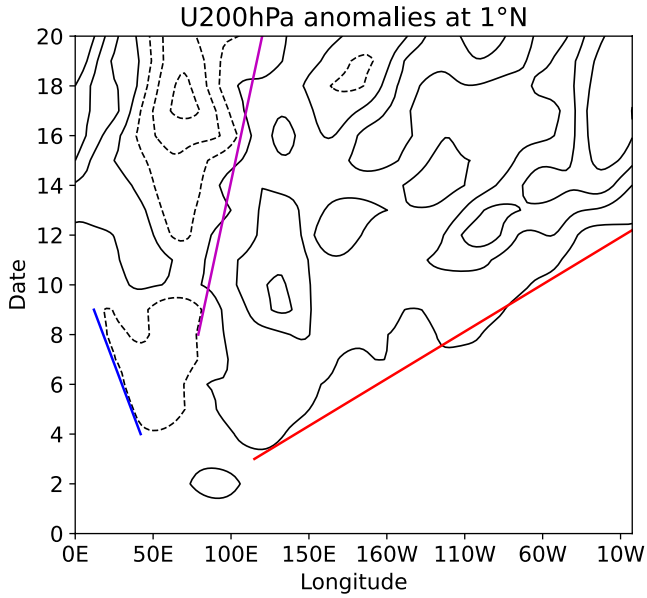

Figure 3. A Hovmöller diagram of zonal wind speed anomalies at 1°N, 200 hPa in the 3K perturbation experiment relative to the Control. The contour interval is 10 m/s, with solid and dashed contour lines starting at ±5 m/s, respectively. The eastward propagating Kelvin wave front is indicated by the red line, the westward propagating Rossby wave front by the blue line, and the excited Madden-Julian oscillation event by the magenta line.

about 8 m/s and 30 m/s, respectively, similar to the speeds in Liang, Fedorov, Zeitlin, and Haertel (2021) but considerably slower than those reported in Jin and Hoskins (1995). The slower speeds presumably result from the coupling between moist convection and equatorial waves, which reduces the equivalent depth of the shallow-water waves (Kiladis et al., 2009). These results again highlight the critical role of the MJO in the moist atmospheric adjustment to a localized heating anomaly in the tropical atmosphere.

3.2. An MSE Budget Analysis

Next, we conduct an moist static energy (MSE) budget analysis to diagnose the mechanisms for the onset and eastward propagation of the excited MJO event. The column integrated MSE tendency in the Control and perturbation experiments can be calculated as follows:

$$\langle \partial h/\partial t \rangle = -\left\langle \frac{u\partial h}{\partial x} \right\rangle - \left\langle \frac{v\partial h}{\partial y} \right\rangle - \left\langle \frac{\omega\partial h}{\partial p} \right\rangle + \langle \mathrm{LW} \rangle + \langle \mathrm{SW} \rangle + \mathrm{LHF} + \mathrm{SHF} + R \tag{2}$$

where $h = c_p T + gZ + L_v q$ is MSE; c_p is dry air heat capacity at constant pressure (1004 J/K/kg); T is temperature; g is the acceleration of gravity taken as 9.8 m/s^2; Z is geopotential height; L_v is latent heat of vaporization (taken constant at 2.5×10^6 J/kg); q is specific humidity; (u, v, ω) are zonal, meridional and vertical pressure velocities, respectively; LW and SW are longwave and shortwave heating rates, respectively; LHF and SHF are surface turbulent latent and sensible heat fluxes, respectively; R is a residual that combines numerical effects, processes that slightly violate MSE conservation, and eddy-scale transports not resolved by the model output data (Andersen & Kuang, 2012); $\langle\rangle$ represents mass-weighted vertical integration from surface to the model top level:

$$\langle x \rangle = \int_{p_{\mathrm{top}}}^{p_{\mathrm{surface}}} x dp/\mathrm{g} \tag{3}$$

Such decomposition has been used in many previous studies where the MSE budget of the MJO was analyzed (e.g., Andersen & Kuang, 2012; Kim et al., 2017; Sobel et al., 2014). In practice, we explicitly calculate $\langle \partial h/\partial t \rangle$ using the 3-hourly model output and use it to calculate the residual term, R, in Equation 2.

The anomalous column integrated MSE tendency in the perturbation experiment relative to the Control can then be calculated as:

$$\langle \partial h/\partial t \rangle' = -\langle u\partial h/\partial x \rangle' - \langle v\partial h/\partial y \rangle' - \langle \omega\partial h/\partial p \rangle' + \langle \mathrm{LW} \rangle' + \langle \mathrm{SW} \rangle' + \mathrm{LHF}' + \mathrm{SHF}' + R' \tag{4}$$

where primes indicate anomalies relative to the Control. $-\langle u\partial h/\partial x \rangle'$, for example, represents the anomalous zonal MSE advection. We then examine how each term on the right-hand-side (RHS) of Equation 4 contributes to the growth and eastward propagation of the anomalous column integrated MSE, $\langle h \rangle'$, used to indicate the excited MJO event in the moisture mode framework (Andersen & Kuang, 2012; Raymond & Fuchs, 2009).

Note that the periods of growth and eastward propagation of the excited MJO are determined using the phase relationship between $\langle \partial h/\partial t \rangle'$ and $\langle h \rangle'$. During the first week, $\langle \partial h/\partial t \rangle'$ is largely in phase with $\langle h \rangle'$, and the MJO amplitude, indicated by $\langle h \rangle'$, gradually increases. The first week therefore corresponds to the MJO growth period. Starting on day 8, $\langle \partial h/\partial t \rangle'$ leads $\langle h \rangle'$ (Figure S5 in Supporting Information S1), and the MJO anomalies propagate eastward. As the equatorially averaged $\langle h \rangle'$ becomes indiscernible after day 18, we define the MJO propagation period from day 8 to day 18. Other methods could also be used to describe the MJO evolution, for example, tracking its precipitation envelope (e.g., Kerns & Chen, 2020; Zhang & Ling, 2017).

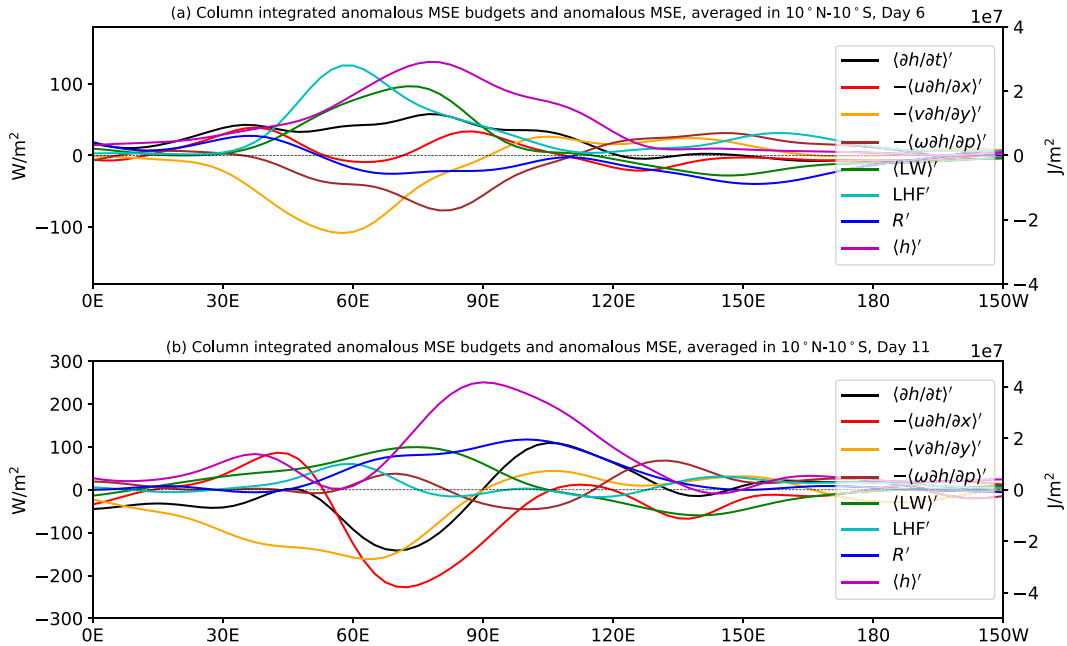

Figure 4. Anomalous moist static energy (MSE) budget terms in Equation 4 averaged between 10°N and 10°S, on (a) day 6 and (b) day 11, in units of W/m^2. The anomalous shortwave heating term, $\langle SW\rangle'$, and the anomalous surface turbulent sensible heat flux term, SHF′, are too small in comparison with the other terms and therefore not plotted. The right vertical axis indicates the computed values for the equatorially averaged anomalous column integrated MSE, $\langle h\rangle'$, shown in magenta.

In Figure 4 we plot the equatorially averaged (10°N–10°S) MSE budget terms in Equation 4 and the anomalous column integrated MSE, $\langle h\rangle'$, on days 6 and 11. These 2 days are representative of the MJO growth and eastward propagation periods, respectively, as will be shown later in Figure 5. Each term is first calculated on the model raw grid and then smoothed. The anomalous shortwave heating, $\langle SW\rangle'$, and the anomalous turbulent sensible heat flux, SHF′, are negligible in comparison with the other terms and therefore not shown. The horizontal structure of each budget term is shown in Figures S6 and S7 in Supporting Information S1.

On day 6, among the three advection terms, $-\langle u\partial h/\partial x\rangle'$ appears to contribute to the growth of $\langle h\rangle'$, due to the advection of relatively moist air (high in MSE, see e.g., Kim et al., 2017; Liang, Fedorov, Zeitlin, & Haertel, 2021) from the Maritime Continent region to the equatorial Indian Ocean by the surface Kelvin-wave easterlies (Figure S4b in Supporting Information S1), while $-\langle v\partial h/\partial y\rangle'$ depletes $\langle h\rangle'$. This is because in the lower troposphere, to the west of the MJO precipitation center, the equatorward flow of two Rossby gyres advects relatively dry air (low in MSE) from the subtropics to the deep tropics, reducing $\langle h\rangle'$, while the poleward flow moistens and recharges the atmospheric column to the east (Figure S6c in Supporting Information S1, see also Adames & Kim, 2016; Ahn et al., 2020; Kim et al., 2017; Liang, Fedorov, Zeitlin, & Haertel, 2021); the discharge of MSE appears to be stronger than the recharge on day 6. The third advection term $-\langle\omega\partial h/\partial p\rangle'$ is collocated with the center of $\langle h\rangle'$ (Figure S6d in Supporting Information S1), which also reduces $\langle h\rangle'$, consistent with the observations that vertical advection exports MSE outside the atmospheric column in the Indo-Pacific warm pool (Back & Bretherton, 2006; Raymond & Fuchs, 2009). The column-integrated anomalous longwave heating, $\langle LW\rangle'$, increases $\langle h\rangle'$, which has been suggested as a key instability mechanism for the MJO (Andersen & Kuang, 2012; Raymond & Fuchs, 2009; Raymond et al., 2009). The enhanced turbulent latent heat flux, LHF′, due to the warm SST perturbation and strong surface westerlies to the west of the MJO precipitation center, recharges $\langle h\rangle'$ (Figure S6f in Supporting Information S1). The residual term, R', is relatively small and hence neglected.

On day 11 (Figure 4b), $\langle\partial h/\partial t\rangle'$ leads $\langle h\rangle'$ by a quarter cycle, and the zonally averaged $\langle\partial h/\partial t\rangle'$ is close to zero, which suggests that the MJO is propagating eastward but not growing in amplitude. The contribution of each term on the RHS of Equation 4 to the maintenance of $\langle h\rangle'$ on day 11 is qualitatively similar to that on day 6, except that $-\langle u\partial h/\partial x\rangle'$ now reduces $\langle h\rangle'$. This appears to result from a much stronger advection of relatively dry air (low in

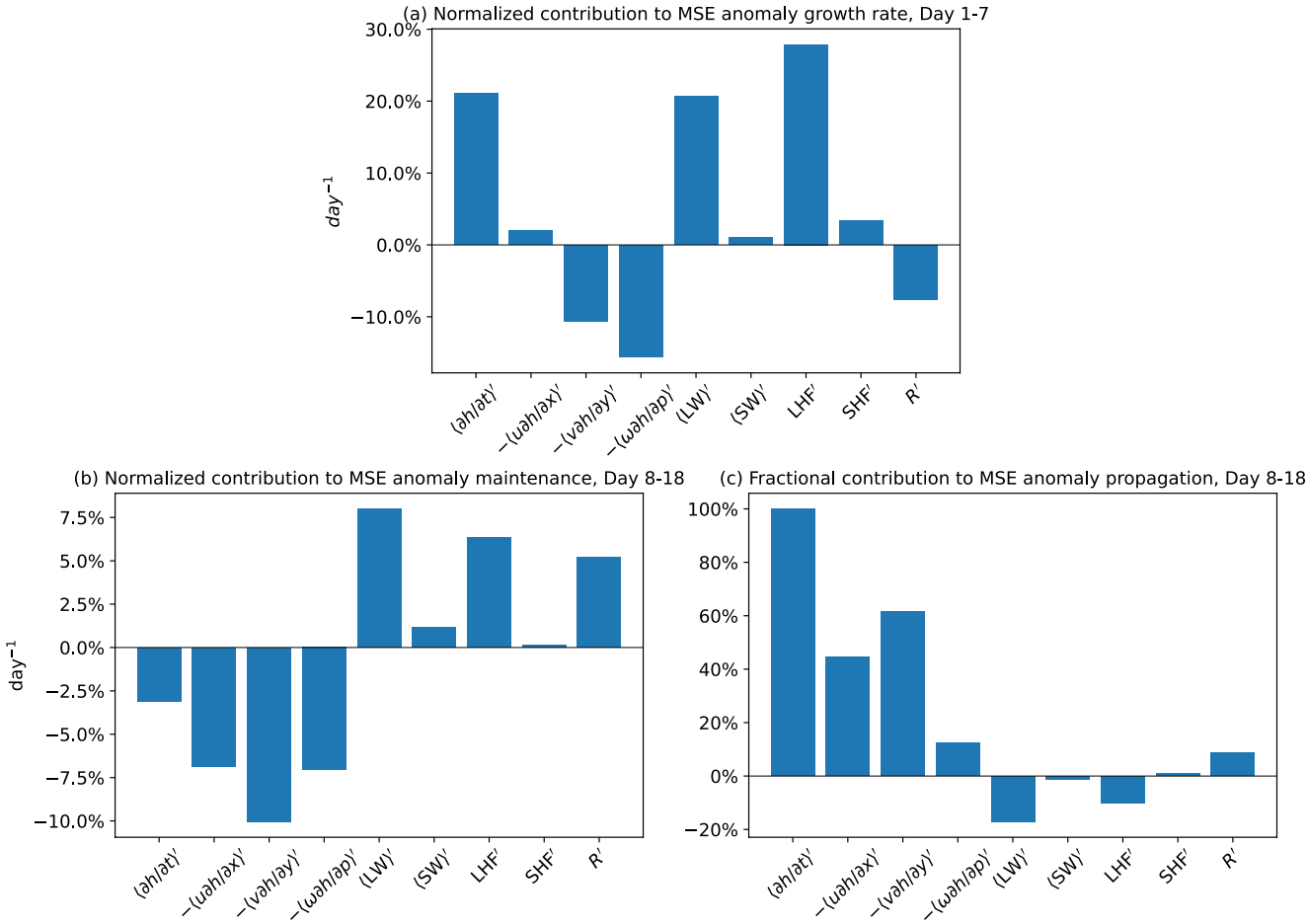

Figure 5. Normalized contribution of each anomalous moist static energy (MSE) budget term in Equation 4 to the (a) growth and (b) maintenance of the excited Madden-Julian oscillation (MJO) event, calculated by projecting the anomalous MSE budget terms onto $\langle h \rangle'$, see Equation 5. (c) Fractional contribution to the eastward propagation of the excited MJO, calculated by projecting each anomalous MSE budget term onto $\langle \partial h/\partial t \rangle'$, see Equation 6.

MSE) from the western equatorial Indian Ocean into the MJO precipitation center by surface westerlies (Figure S7b in Supporting Information S1). Note that the residual term, R', is greater on day 11 than on day 6, likely due to the generally larger magnitude of the budget terms, assuming that the magnitude of numerical errors is the same. Overall, as one can see later in Figures 5a and 5b, the normalized contribution of R' to the maintenance of $\langle h \rangle'$ between days 8 and 18 is even slightly smaller than that during the first week.

In the context of the eastward propagation of the MJO, $-\langle u\partial h/\partial x \rangle'$ and $-\langle v\partial h/\partial y \rangle'$, as discussed before, recharge $\langle h \rangle'$ to the east of the MJO precipitation center and discharge $\langle h \rangle'$ to the west, therefore contributing to the MJO's eastward propagation. $-\langle \omega\partial h/\partial p \rangle'$ is the major source of MSE buildup at the leading edge of the MJO precipitation, which also favors the MJO's eastward propagation. This vertical advection process has been related to cumulus congestus clouds, which are forecd by the boundary layer convergence and moisten the mid-troposphere (Kiladis et al., 2009; Liang, Fedorov, Zeitlin, & Haertel, 2021; Wang & Rui, 1990). The positive $\langle \mathrm{LW} \rangle'$ due to the MJO stratiform clouds (Kiladis et al., 2009), and the enhanced LHF′, both lag the MJO precipitation center and therefore disfavor the eastward propagation. Note that the magnitude of LHF′ is quite small now, likely due to the warm SST perturbation being turned off.

The residual term, R', appears to be the leading contributor to the positive MSE tendency to the east of the MJO convection center on day 11. However, since it recharges $\langle h \rangle'$ to the west of the MJO convection center at the same time, overall its contribution to the eastward propagation of the excited MJO is relatively small compared to the MSE advection terms. Moreover, as we show in Figure S8 in Supporting Information S1, on other days the

contribution of R' to the positive MSE tendency to the east of the convection center is much smaller or even negative. For example, on day 10 the contribution of R' to the positive MSE tendency is smaller than $-\langle v\partial h/\partial y\rangle'$, $-\langle \omega\partial h/\partial p\rangle'$, and LHF′; on days 12 and 13, R' even lags $\langle h\rangle'$, acting against the eastward propagation of the MJO.

One way to better quantify the contribution of each budget term in Equation 4 to the MJO growth, maintenance and eastward propagation is to project them onto the MJO MSE anomaly, $\langle h\rangle'$, and its time derivative, $\langle \partial h/\partial t\rangle'$ (Andersen & Kuang, 2012). Figure 5a shows the normalized contribution C_x of each budget term x to the growth rate of $\langle h\rangle'$ during the first week, calculated as:

$$C_x = \frac{\|x.\langle h\rangle'\|}{\|\langle h\rangle'^2\|}, \tag{5}$$

where $\|y\| = \int_t \iint_{eq} y dA dt$ is the integral in space over the equatorial Indo-Western Pacific (10°N–10°S, 45°E−180°), and in time over the first week. The average normalized growth rate of the excited MJO, $C_{\langle \partial h/\partial t\rangle'}$, is about 20% day^{-1} (Figure 5a). Consistent with the analysis on day 6, $\langle \mathrm{LW}\rangle'$ and LHF′ are the main contributors to the MJO growth in the first week, while $-\langle v\partial h/\partial y\rangle'$ and $-\langle \omega\partial h/\partial p\rangle'$ are the two main factors for reducing the MJO growth.

Similarly, the average normalized growth rate of the excited MJO event between days 8 and 18 can be calculated as −3% day^{-1} (Figure 5b), which is much smaller than that during the MJO growing period. This suggests that the excited MJO event barely maintains its amplitude while propagating eastward after the first week. Note that between days 13 and 18, we slightly narrow the zonal integral region to 75°E−180°, due to an eastward shift of the MJO precipitation center. The top two contributors to the MJO maintenance are $\langle \mathrm{LW}\rangle'$ and LHF′, the same as during the MJO growing period, while the three advection terms, all deplete $\langle h\rangle'$ and cause the decay of the MJO.

The fractional contribution c_x of each budget term to the eastward propagation of the MJO, as indicated by $\langle \partial h/\partial t\rangle'$, between days 8 and 18, can be similarly calculated as:

$$c_x = \frac{\|x.\langle \partial h/\partial t\rangle'\|}{\|\langle \partial h/\partial t\rangle'^2\|}, \tag{6}$$

The results are shown in Figure 5c. Consistent with the analysis on day 11, all three components of the anomalous MSE advection contribute to the eastward propagation of the excited MJO event, with the vertical component playing a relatively minor role; $\langle \mathrm{LW}\rangle'$ and LHF′, on the other hand, oppose the MJO's eastward propagation.

4. Summary and Discussion

In this study, using SPCAM, we simulate the excitation of a primary MJO event (i.e., not preceded by a previous event, see Matthews, 2008) in response to an idealized transient Gaussian-shape warm SST perturbation in the Indian Ocean, whose maximum magnitude is 3K. The excited MJO event builds up its strength over the warm SST perturbation in the central-eastern equatorial Indian Ocean in the first week, then propagates eastward at a speed of about 6 m/s across the Maritime Continent, reaches the West Pacific, and finally dissipates. Similar results are obtained when the same transient SST perturbation is added during other MJO-inactive periods in the Control experiment (Figures S9 and S10 in Supporting Information S1), but the amplitude of the excited MJO events varies from one experiment to the next. This study confirms the conclusion of Liang, Fedorov, Zeitlin, and Haertel (2021), who used a Lagrangian atmospheric GCM (Haertel et al., 2014, 2017), that in addition to equatorial Rossby and Kelvin waves, the MJO can play an important role in the moist adjustment of the tropical atmosphere to localized equatorial ocean heating (Figure 3).

A MSE budget analysis is utilized to diagnose the mechanisms for the onset and eastward propagation of the excited MJO event. We find that during the first week, the enhanced turbulent latent heat flux and longwave heating contribute most to the MJO growth, the latter of which has been suggested as one of the key instability mechanisms for the MJO (Andersen & Kuang, 2012; Raymond & Fuchs, 2009; Raymond et al., 2009). The anomalous meridional and vertical advection of MSE, on the other hand, deplete the column-integrated MSE anomaly and weaken the MJO growth. Between days 8 and 18, when the MJO propagates eastward, the enhanced turbulent latent heat flux and longwave heating similarly help maintain the MJO amplitude, while the anomalous

advection of MSE reduces it. Nevertheless, the anomalous advection of MSE is found to play the dominant role in the eastward propagation of the excited MJO, consistent with other studies (e.g., Andersen & Kuang, 2012; Kim et al., 2017; Sobel et al., 2014), while the anomalous turbulent latent heat flux and longwave heating oppose it.

We note that the current MSE budget analysis is based on an MJO event excited by an imposed SST anomaly, and should not be necessarily generalized as the only mechanisms for MJO generation and propagation. For example, in Andersen and Kuang (2012), who used an older version of SPCAM to simulate the MJO, the vertical advection of MSE, although weaker than the effects of the horizontal advection, played a rather important role in the eastward propagation of the MJO.

That a primary MJO event can be triggered by SST warming in the equatorial Indian Ocean may have implications for the MJO prediction, although Matthews (2008) found no clear composite warm SST signals before the primary MJO event initiation, possibly because the MJO has other generation mechanisms as well. The sea surface warming of 1–3 K before the initiation of a successive event, due to reduced surface latent heat flux and enhanced short-wave radiation flux anomalies (DeMott et al., 2015; Flatau et al., 1997; Moum et al., 2014; Shinoda et al., 1998), however, is often observed. We propose that SPCAM is well suited to investigate how low-level atmospheric stability and free-troposphere moisture, before the initiation of a successive event, regulate the convective response to SST fluctuations during the MJO cycle (DeMott et al., 2015; Jiang et al., 2020). Moreover, such idealized experiment as in the current study, can serve as a test bed for simple models of the MJO (e.g., Rostami & Zeitlin, 2020; Vallis, 2021), where moist convection, critical for the MJO dynamics, is usually treated in a relatively crude way.

Data Availability Statement

This study is based on the model output from the Super-Parameterized CAM (SPCAM) of the NCAR Community Earth System Model version 2.1.0 (CESM2) (Danabasoglu et al., 2020). CESM2 is publicly available at https://www.cesm.ucar.edu/models/cesm2/. The model output is archived in Dryad (https://doi.org/10.5061/dryad.h44j0zpnx).

Acknowledgments
Yu Liang acknowledges the computing resources provided by the Yale center for research computing. This research has been supported in part by grants to Alexey V. Fedorov from NASA (80NSSC18K1396) and NOAA (NA20OAR4310377). The authors acknowledge two anonymous reviewers who helped improve this paper.

References

Adames, Á. F., & Kim, D. (2016). The MJO as a dispersive, convectively coupled moisture wave: Theory and observations. *Journal of the Atmospheric Sciences*, *73*(3), 913–941. https://doi.org/10.1175/jas-d-15-0170.1

Ahn, M.-S., Kim, D., Kang, D., Lee, J., Sperber, K. R., Gleckler, P. J., et al. (2020). MJO propagation across the maritime continent: Are CMIP6 models better than CMIP5 models? *Geophysical Research Letters*, *47*(11), e2020GL087250. https://doi.org/10.1029/2020gl087250

Andersen, J. A., & Kuang, Z. (2012). Moist static energy budget of MJO-like disturbances in the atmosphere of a zonally symmetric aquaplanet. *Journal of Climate*, *25*(8), 2782–2804. https://doi.org/10.1175/jcli-d-11-00168.1

Back, L., & Bretherton, C. (2006). Geographic variability in the export of moist static energy and vertical motion profiles in the tropical Pacific. *Geophysical Research Letters*, *33*(17), L17810. https://doi.org/10.1029/2006gl026672

Danabasoglu, G., Lamarque, J.-F., Bacmeister, J., Bailey, D., DuVivier, A., Edwards, J., et al. (2020). The community Earth system model version 2 (CESM2). *Journal of Advances in Modeling Earth Systems*, *12*(2), e2019MS001916. https://doi.org/10.1029/2019ms001916

DeMott, C. A., Klingaman, N. P., & Woolnough, S. J. (2015). Atmosphere-ocean coupled processes in the Madden-Julian oscillation. *Reviews of Geophysics*, *53*(4), 1099–1154. https://doi.org/10.1002/2014rg000478

Flatau, M., Flatau, P. J., Phoebus, P., & Niiler, P. P. (1997). The feedback between equatorial convection and local radiative and evaporative processes: The implications for intraseasonal oscillations. *Journal of the Atmospheric Sciences*, *54*(19), 2373–2386. https://doi.org/10.1175/1520-0469(1997)054<2373:tfbeca>2.0.co;2

Gill, A. E. (1980). Some simple solutions for heat-induced tropical circulation. *Quarterly Journal of the Royal Meteorological Society*, *106*(449), 447–462. https://doi.org/10.1002/qj.49710644905

Haertel, P. (2020). Kelvin/Rossby wave partition of Madden-Julian oscillation circulations. *Climate*, *9*(1), 2. https://doi.org/10.3390/cli9010002

Haertel, P., Boos, W., & Straub, K. (2017). Origins of moist air in global Lagrangian simulations of the Madden–Julian Oscillation. *Atmosphere*, *8*(9), 158. https://doi.org/10.3390/atmos8090158

Haertel, P., Straub, K., & Fedorov, A. (2014). Lagrangian overturning and the Madden–Julian oscillation. *Quarterly Journal of the Royal Meteorological Society*, *140*(681), 1344–1361. https://doi.org/10.1002/qj.2216

Hannah, W. M., Maloney, E. D., & Pritchard, M. S. (2015). Consequences of systematic model drift in DYNAMO MJO hindcasts with SP-CAM and CAM5. *Journal of Advances in Modeling Earth Systems*, *7*(3), 1051–1074. https://doi.org/10.1002/2014ms000423

Heckley, W., & Gill, A. (1984). Some simple analytical solutions to the problem of forced equatorial long waves. *Quarterly Journal of the Royal Meteorological Society*, *110*(463), 203–217. https://doi.org/10.1002/qj.49711046314

Hendon, H. H., & Liebmann, B. (1990). The intraseasonal (30–50 day) oscillation of the Australian summer monsoon. *Journal of the Atmospheric Sciences*, *47*(24), 2909–2924. https://doi.org/10.1175/1520-0469(1990)047<2909:tidoot>2.0.co;2

Higgins, R., Schemm, J. E., Shi, W., & Leetmaa, A. (2000). Extreme precipitation events in the Western United States related to tropical forcing. *Journal of Climate*, *13*(4), 793–820. https://doi.org/10.1175/1520-0442(2000)013<0793:epeitw>2.0.co;2

Jiang, X., Adames, Á. F., Kim, D., Maloney, E. D., Lin, H., Kim, H., et al. (2020). Fifty years of research on the Madden-Julian oscillation: Recent progress, challenges, and perspectives. *Journal of Geophysical Research: Atmospheres*, *125*(17), e2019JD030911. https://doi.org/10.1029/2019jd030911

Jin, F., & Hoskins, B. J. (1995). The direct response to tropical heating in a baroclinic atmosphere. *Journal of the Atmospheric Sciences*, *52*(3), 307–319. https://doi.org/10.1175/1520-0469(1995)052<0307:tdrtth>2.0.co;2

Jones, C., Waliser, D. E., Lau, K., & Stern, W. (2004). Global occurrences of extreme precipitation and the Madden–Julian oscillation: Observations and predictability. *Journal of Climate*, *17*(23), 4575–4589. https://doi.org/10.1175/3238.1

Kerns, B. W., & Chen, S. S. (2020). A 20-year climatology of Madden-Julian oscillation convection: Large-scale precipitation tracking from TRMM-GPM rainfall. *Journal of Geophysical Research: Atmospheres*, *125*(7), e2019JD032142. https://doi.org/10.1029/2019jd032142

Kessler, W. S., & Kleeman, R. (2000). Rectification of the Madden–Julian oscillation into the ENSO cycle. *Journal of Climate*, *13*(20), 3560–3575. https://doi.org/10.1175/1520-0442(2000)013<3560:rotmjo>2.0.co;2

Khairoutdinov, M. F., & Randall, D. A. (2001). A cloud resolving model as a cloud parameterization in the NCAR community climate system model: Preliminary results. *Geophysical Research Letters*, *28*(18), 3617–3620. https://doi.org/10.1029/2001gl013552

Khairoutdinov, M. F., & Randall, D. A. (2003). Cloud resolving modeling of the arm summer 1997 iop: Model formulation, results, uncertainties, and sensitivities. *Journal of the Atmospheric Sciences*, *60*(4), 607–625. https://doi.org/10.1175/1520-0469(2003)060<0607:crmota>2.0.co;2

Kiladis, G. N., Straub, K. H., & Haertel, P. T. (2005). Zonal and vertical structure of the Madden–Julian oscillation. *Journal of the Atmospheric Sciences*, *62*(8), 2790–2809. https://doi.org/10.1175/jas3520.1

Kiladis, G. N., Wheeler, M. C., Haertel, P. T., Straub, K. H., & Roundy, P. E. (2009). Convectively coupled equatorial waves. *Reviews of Geophysics*, *47*(2), RG2003. https://doi.org/10.1029/2008rg000266

Kim, D., Kim, H., & Lee, M.-I. (2017). Why does the MJO detour the maritime continent during austral summer? *Geophysical Research Letters*, *44*(5), 2579–2587. https://doi.org/10.1002/2017gl072643

Kim, H., Vitart, F., & Waliser, D. E. (2018). Prediction of the Madden–Julian Oscillation: A review. *Journal of Climate*, *31*(23), 9425–9443. https://doi.org/10.1175/jcli-d-18-0210.1

Klingaman, N. P., Woolnough, S. J., Jiang, X., Waliser, D., Xavier, P. K., Petch, J., et al. (2015). Vertical structure and physical processes of the Madden-Julian oscillation: Linking hindcast fidelity to simulated diabatic heating and moistening. *Journal of Geophysical Research: Atmospheres*, *120*(10), 4690–4717. https://doi.org/10.1002/2014jd022374

Lau, K.-M., & Phillips, T. J. (1986). Coherent fluctuations of extratropical geopotential height and tropical convection in intraseasonal time scales. *Journal of the Atmospheric Sciences*, *43*(11), 1164–1181. https://doi.org/10.1175/1520-0469(1986)043<1164:cfofgh>2.0.co;2

Li, T., Zhao, C., Hsu, P.-C., & Nasuno, T. (2015). MJO initiation processes over the tropical Indian Ocean during dynamo/Cindy 2011. *Journal of Climate*, *28*(6), 2121–2135. https://doi.org/10.1175/jcli-d-14-00328.1

Liang, Y., & Fedorov, A. V. (2021). Linking the Madden–Julian Oscillation, tropical cyclones and westerly wind bursts as part of El Niño development. *Climate Dynamics*, *57*(3), 1039–1060. https://doi.org/10.1007/s00382-021-05757-1

Liang, Y., Fedorov, A. V., & Haertel, P. (2021). Intensification of westerly wind bursts caused by the coupling of the Madden-Julian oscillation to SST during El Niño onset and development. *Geophysical Research Letters*, *48*(9), e2020GL089395. https://doi.org/10.1029/2020gl089395

Liang, Y., Fedorov, A. V., Zeitlin, V., & Haertel, P. (2021). Excitation of the Madden–Julian oscillation in atmospheric adjustment to equatorial heating. *Journal of the Atmospheric Sciences*, *78*(12), 3933–3950.

Liebmann, B., Hendon, H. H., & Glick, J. D. (1994). The relationship between tropical cyclones of the Western Pacific and Indian Oceans and the Madden-Julian oscillation. *Journal of the Meteorological Society of Japan. Series II*, *72*(3), 401–412. https://doi.org/10.2151/jmsj1965.72.3_401

Madden, R. A., & Julian, P. R. (1972). Description of global-scale circulation cells in the tropics with a 40–50 day period. *Journal of the Atmospheric Sciences*, *29*(6), 1109–1123. https://doi.org/10.1175/1520-0469(1972)029<1109:dogscc>2.0.co;2

Maloney, E. D., & Hartmann, D. L. (2000). Modulation of eastern north Pacific hurricanes by the Madden–Julian oscillation. *Journal of Climate*, *13*(9), 1451–1460. https://doi.org/10.1175/1520-0442(2000)013<1451:moenph>2.0.co;2

Matsuno, T. (1966). Quasi-geostrophic motions in the equatorial area. *Journal of the Meteorological Society of Japan. Series II*, *44*(1), 25–43. https://doi.org/10.2151/jmsj1965.44.1_25

Matthews, A. J. (2008). Primary and successive events in the Madden–Julian oscillation. *Quarterly Journal of the Royal Meteorological Society: A journal of the atmospheric sciences, applied meteorology and physical oceanography*, *134*(631), 439–453. https://doi.org/10.1002/qj.224

McPhaden, M. J. (1999). Genesis and evolution of the 1997–1998 El Niño. *Science*, *283*(5404), 950–954. https://doi.org/10.1126/science.283.5404.950

Moum, J. N., de Szoeke, S. P., Smyth, W. D., Edson, J. B., DeWitt, H. L., Moulin, A. J., et al. (2014). Air–sea interactions from westerly wind bursts during the November 2011 MJO in the Indian Ocean. *Bulletin of the American Meteorological Society*, *95*(8), 1185–1199. https://doi.org/10.1175/bams-d-12-00225.1

Nakajima, K., Toyoda, E., Ishiwatari, M., Takehiro, S.-I., & Hayashi, Y.-Y. (2004). Initial development of tropical precipitation patterns in response to a local warm SST area: An aqua-planet ensemble study. *Journal of the Meteorological Society of Japan. Series II*, *82*(6), 1483–1504. https://doi.org/10.2151/jmsj.82.1483

Rasp, S., Pritchard, M. S., & Gentine, P. (2018). Deep learning to represent subgrid processes in climate models. *Proceedings of the National Academy of Sciences of the United States of America*, *115*(39), 9684–9689. https://doi.org/10.1073/pnas.1810286115

Raymond, D. J. (2001). A new model of the Madden–Julian Oscillation. *Journal of the Atmospheric Sciences*, *58*(18), 2807–2819. https://doi.org/10.1175/1520-0469(2001)058<2807:anmotm>2.0.co;2

Raymond, D. J., & Fuchs, Z. (2009). Moisture modes and the Madden–Julian Oscillation. *Journal of Climate*, *22*(11), 3031–3046. https://doi.org/10.1175/2008jcli2739.1

Raymond, D. J., Sessions, S. L., Sobel, A. H., & Fuchs, Z. (2009). The mechanics of gross moist stability. *Journal of Advances in Modeling Earth Systems*, *1*(3). https://doi.org/10.3894/james.2009.1.9

Rostami, M., & Zeitlin, V. (2020). Can geostrophic adjustment of baroclinic disturbances in tropical atmosphere explain MJO events? *Quarterly Journal of the Royal Meteorological Society*, *146*(733), 3998–4013. https://doi.org/10.1002/qj.3884

Rydbeck, A. V., & Jensen, T. G. (2017). Oceanic impetus for convective onset of the Madden–Julian oscillation in the Western Indian ocean. *Journal of Climate*, *30*(11), 4299–4316. https://doi.org/10.1175/jcli-d-16-0595.1

Shinoda, T., Hendon, H. H., & Glick, J. (1998). Intraseasonal variability of surface fluxes and sea surface temperature in the tropical Western Pacific and Indian oceans. *Journal of Climate*, *11*(7), 1685–1702. https://doi.org/10.1175/1520-0442(1998)011<1685:ivosfa>2.0.co;2

Sobel, A., & Maloney, E. (2013). Moisture modes and the eastward propagation of the MJO. *Journal of the Atmospheric Sciences*, *70*(1), 187–192. https://doi.org/10.1175/jas-d-12-0189.1

Sobel, A., Wang, S., & Kim, D. (2014). Moist static energy budget of the MJO during DYNAMO. *Journal of the Atmospheric Sciences*, *71*(11), 4276–4291. https://doi.org/10.1175/jas-d-14-0052.1

Stan, C. (2018). The role of SST variability in the simulation of the MJO. *Climate Dynamics*, *51*(7), 2943–2964. https://doi.org/10.1007/s00382-017-4058-2

Vallis, G. K. (2021). Distilling the mechanism for the Madden–Julian oscillation into a simple translating structure. *Quarterly Journal of the Royal Meteorological Society*, *147*(738), 3032–3047. https://doi.org/10.1002/qj.4114

Waliser, D. (2005). Predictability and forecasting. In *Intraseasonal variability in the atmosphere-ocean climate system* (pp. 389–423). Springer.

Wang, B., & Rui, H. (1990). Dynamics of the coupled moist Kelvin–Rossby wave on an equatorial beta-plane. *Journal of the Atmospheric Sciences*, *47*(4), 397–413. https://doi.org/10.1175/1520-0469(1990)047<0397:dotcmk>2.0.co;2

Wheeler, M., & Kiladis, G. N. (1999). Convectively coupled equatorial waves: Analysis of clouds and temperature in the wavenumber–frequency domain. *Journal of the Atmospheric Sciences*, *56*(3), 374–399. https://doi.org/10.1175/1520-0469(1999)056<0374:ccewao>2.0.co;2

Woolnough, S. J., Slingo, J. M., & Hoskins, B. J. (2001). The organization of tropical convection by intraseasonal sea surface temperature anomalies. *Quarterly Journal of the Royal Meteorological Society*, *127*(573), 887–907. https://doi.org/10.1002/qj.49712757310

Yanai, M., Esbensen, S., & Chu, J.-H. (1973). Determination of bulk properties of tropical cloud clusters from large-scale heat and moisture budgets. *Journal of the Atmospheric Sciences*, *30*(4), 611–627. https://doi.org/10.1175/1520-0469(1973)030<0611:dobpot>2.0.co;2

Zhang, C. (2005). Madden-Julian oscillation. *Reviews of Geophysics*, *43*(2). https://doi.org/10.1029/2004rg000158

Zhang, C., & Ling, J. (2017). Barrier effect of the Indo-Pacific maritime continent on the MJO: Perspectives from tracking MJO precipitation. *Journal of Climate*, *30*(9), 3439–3459. https://doi.org/10.1175/jcli-d-16-0614.1

Zhao, C., Li, T., & Zhou, T. (2013). Precursor signals and processes associated with MJO initiation over the tropical Indian Ocean. *Journal of Climate*, *26*(1), 291–307. https://doi.org/10.1175/jcli-d-12-00113.1